Sigma J Eng Nat Sci, Vol. 41, No. 1, pp. 119–129, February, 2023

Sigma Journal of Engineering and Natural Sciences
Web page info: https://sigma.yildiz.edu.tr
DOI: 10.14744/sigma.2023.00012

Research Article

Fusion and CNN based classification of liver focal lesions using magnetic resonance imaging phases

Mücahit CİHAN[1,*], Betül UZBAŞ[2], Murat CEYLAN[1]

[1]Department of Electrical and Electronics Engineering, Konya Technical University, Konya, 42250, Türkiye
[2]Department of Computer Engineering, Konya Technical University, Konya,42250, Türkiye

ARTICLE INFO

Article history
Received: 21 April 2021
Accepted: 08 July 2021

Keywords:
Fusion; Convolutional Neural Networks; Discrete Wavelet Transform; Segmentation; Liver Lesion Classification

ABSTRACT

The diagnosis and follow-up of focal liver lesions have an important place in radiology practice and in planning the treatment of patients. Lesions detected in the liver can be benign or malign. While benign lesions do not require any treatment, some treatments and surgical operations may be required for malign lesions. Magnetic resonance imaging provides some advantages over other imaging modalities in the detection and characterization of focal liver lesions with its superior soft tissue contrast. Additionally, different phases help make a clear diagnosis of different contrast agent retention properties in magnetic resonance imaging. This study aims to classify focal liver lesions based on convolutional neural networks by fusing magnetic resonance liver images obtained in pre-contrast, venous, arterial, and delayed phases. Magnetic resonance imaging data were obtained from Selcuk University, Faculty of Medicine, Department of Radiology in Turkey. The experiments were performed using 460 magnetic resonance images in four phases of 115 patients. Two experiments were conducted. Two-dimensional discrete wavelet transform was used to fuse the phases in both experiments. In the first experiment, the best model was determined using the original data, different number of convolution layers and different activation functions. In the second experiment, the best-found model was used. Additionally, the number of data was increased using data augmentation methods in this experiment. The results were compared with other state-of-the art methods and the superiority of the proposed method was proved. As a result of the classification, 96.66% accuracy, 86.67% sensitivity and 98.76% specificity rates were obtained. When the results are examined, CNN efficiency increases by fusing MR liver images taken in different phases.

Cite this article as: Cihan M, Uzbaş B, Ceylan M. Fusion and CNN based classification of liver focal lesions using magnetic resonance imaging phases.Sigma J Eng Nat Sci 2023;41(1):119–129.

***Corresponding author.**
*E-mail address: mcihan@ktun.edu.tr

This paper was recommended for publication in revised form by Regional Editor N. Özlem Ünverdi

Published by Yıldız Technical University Press, İstanbul, Turkey

INTRODUCTION

Focal lesions are very common in the liver. The majority of these lesions are benign (simple cyst, hemangioma), while some are malign (cholangiocarcinoma, metastasis). Identification and differential diagnosis of liver focal lesions are very critical for treatment planning. Radiographic imaging plays an important role in reducing cancer mortality, especially Computer Tomography (CT) and Magnetic Resonance Imaging (MRI) the methods used to aid in liver tumor diagnosis [1]. In medical imaging, when a liver lesion is detected by radiographic imaging, a radiologist will need to understand whether the nature and type of liver lesion is malign or benign [2].

MRI is a medical imaging method commonly used in radiology to create images of the body's anatomy and physiological processes. Liver MRI is used many times in the detection of focal liver lesions and in the evaluation of common liver diseases [3-6]. MRI has many advantages compared to CT, such as the lack of ionizing radiation and better lesion detection [7]. In addition, MR images in different phases provide differential diagnostic evaluations for liver lesions. The features obtained in the T1 and T2 phases affect the contrast of the images in different phases and provide quantitative information about the lesions [8]. In this study, one of the multiresolution analysis methods, Wavelet Transform (WT), was used to extract numerical features from MR liver images.

Multiresolution Analysis methods have become very popular, especially with the development of wavelets. Multiresolution analysis methods that capture different features of images at various scales are widely used in image processing applications [9]. Multiresolution concerns with the display and analysis of images in different resolutions. Inconspicuous features at one level can be easily detected at another. Multiresolution analysis is based on WT [10]. WT was used in medical images for the first time in the study by Mojsilovic et al. [11]. Beura et al. [12] and Uppal [13] used WT to detect breast cancer, while Sarhan [14] used it to classify brain tumors. There are also studies conducted to detect liver tumor [8, 15].

Convolutional Neural Networks (CNN) is a neural network consisting of an input layer, output layer and multiple hidden layers, which are often preferred for image classification applications. Many biomedical studies have been classified using CNN [16, 17]. For example, Alakwaa et al. [18] detected lung cancer using a 3D CNN. Alkhaleefah and Wu [19] classified mammograms using a hybrid CNN and Support Vector Machines approach. Frid-Adar et al. [20] increased the performance of CNN in the classification of liver lesions by generating synthetic images with Generative Adversarial Networks (GAN). Kabe et al. [1] proposed a classification of four types of liver lesions using convolutional neural networks with a succinct model called FireNet. To prevent overfitting while training CNN, researchers have used many effective tricks, including activation functions [21], dropout layers [22], and data augmentation [23].

This study focuses on classifying benign and malign tumors with the most advanced deep learning-based techniques by fusing MR liver images in different phases. Initially, MR liver images obtained in 4 different phases from 115 patients were segmented manually with the help of radiologists. The phases of the segmented images were decomposed into sub-bands by 2D DWT and fused using the maximum selection rule. CNN was used as the classifier. Accuracy, sensitivity and specificity values were calculated to evaluate the performance of the proposed method. Two separate experiments were conducted, and the results of the experiments were compared with state-of-the art methods. As a result of this comparison, the efficiency of the proposed method was proven.

PROPOSED METHODOLOGY

The proposed methodology consists of four important stages, namely, liver segmentation, feature extraction using 2D DWT, image fusion and rules and classification using the Convolutional Neural Networks (CNNs). The overall block diagram of the proposed scheme is shown in Figure 1. As shown, initially the liver segmentation was made with the help of expert radiologists. Then, the approximation and detail coefficients were extracted using the level-2 2D DWT. The coefficients obtained for different phases were segmented with the maximum selection rule and fused images were created. Finally, the fused images are classified by the CNN classifier. All four stages are discussed below in detail.

Segmentation

Segmentation is a pre-process performed in order to separate the relevant image structure from the ground and other image components. It is usually the first step of image analysis, and is of great importance for image processing applications. The segmentation success directly affects the success of the analysis process.

In medical image processing applications; when differentiating tumor, mass etc., it is important to detect organs such as the heart, liver and brain from MR images [24]. This is because MR images contain unnecessary details that do not contribute to lesion detection. These details can cause the mathematical methods that try interpreting the lesions using the pixel values to produce incorrect results. Therefore, to make a more accurate diagnosis, only the region of interest should be selected from the MR images. Unnecessary details in the MR liver images used in this study were eliminated by the segmentation process performed by expert radiologists. The liver segmentation was carried out manually using expert knowledge. The expert encircles his/her region of interest and thus more optimum

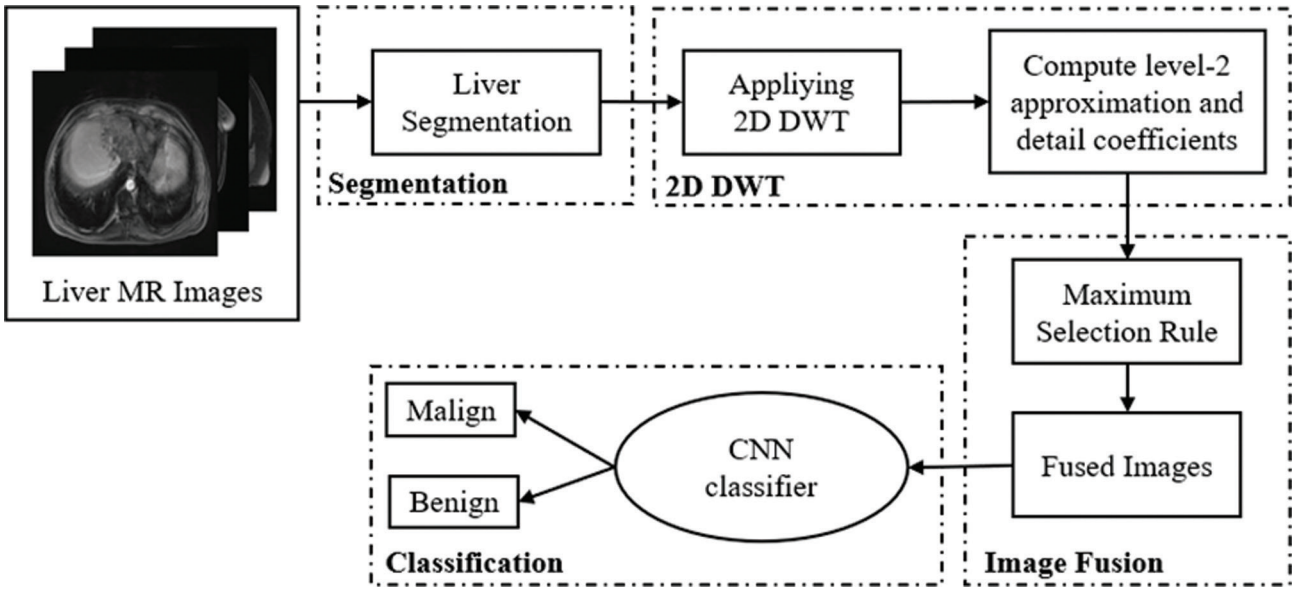

Figure 1. Block diagram of the proposed method for MR liver image Classification.

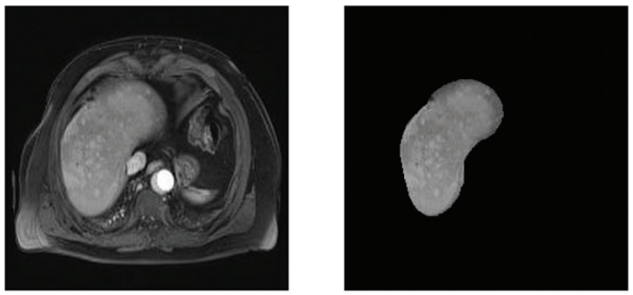

Figure 2. Segmentation: (a) original MR liver image, (b) segmented image.

results are obtained. The image obtained by applying segmentation to a sample MR liver image is shown in Figure 2.

2D Discrete Wavelet Transform (2D DWT)

Wavelet Transform (WT) is an effective tool used for image analysis methods. WT is a method that examines each component at a resolution suitable for its scale by dividing the data into different frequency components. One of its biggest advantages is that it allows local analysis. In this way, large signals can be analyzed in a small area.

The wavelet function family is obtained by shifting and scaling the mother wavelet function. Let $f(x)$ be a continuous, square-integrable function. The continuous wavelet transform of $f(x)$ with respect to Ψ(x), which is a real-valued wavelet, is defined as [25],

$$W_{\psi(a,b)} = \int_{-\infty}^{+\infty} f(x)\psi_{a,b}(x)dx \qquad (1)$$

where

$$\psi_{a,b}(x) = \frac{1}{\sqrt{a}}\psi\left(\frac{x-b}{a}\right);\ a \in \Re^{+},\ b \in \Re \qquad (2)$$

with a and b being scaled and translation parameters, respectively. The wavelet function $\Psi_{a,b}(x)$ is constructed from the mother wavelet Ψ(.) using a and b. The discrete variation of Equation 1 can be obtained by restraining a and b to a discrete lattice with $a = 2^j$ and $a = 2^j k$ and is expressed as,

$$DWT_{f(n)} = \begin{cases} A_{i,j}(n) = \sum_n f(n) L_i^*\left(n - 2^i j\right) \\ D_{i,j}(n) = \sum_n f(n) H_i^*\left(n - 2^i j\right) \end{cases} \qquad (3)$$

where $A_{i,j}(n)$ refers to the coefficients of the approximation component and $D_{i,j}(n)$ denotes the coefficients of the detail components. The functions $L(n)$ and $H(n)$ represent the coefficients of low-pass and high-pass filters, respectively. Two parameters i and j represent the wavelet scale and translation factors, respectively. Using a combination of these digital filters and down-samplers, a 2D DWT is applied. Figure 3 shows the 2D DWT analysis process using filter banks. In the case of images, DWT is applied to each dimension individually, that is, the rows and columns of the image are passed through 1D DWT individually to create the 2D DWT. As a result, four sub-band images (LL: low-low, LH: low-high, HL: high-low, HH: high-high) are obtained at each level. Among them, the three sub-band images LH (D_i^h), HL (D_i^v), HH (D_i^d) are detail images in the horizontal, vertical and diagonal directions, respectively. The LL (A_i) sub-band is the approximation image used for

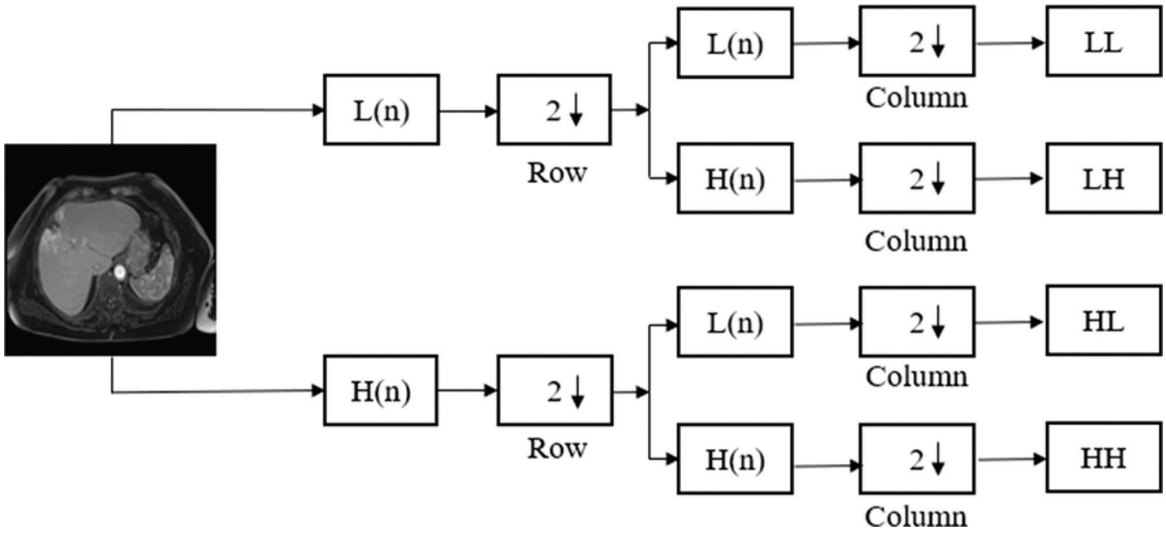

Figure 3. 2D DWT analysis using filter banks.

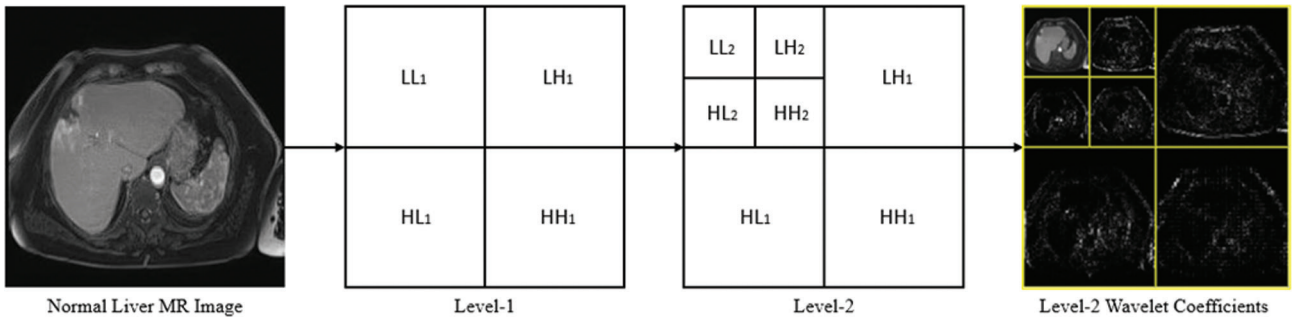

Figure 4. Level-2 decomposition and obtained wavelet coefficients for 2D DWT.

the next level 2D DWT calculations. Also, Figure 4 shows the level-2 decomposition process and the wavelet coefficients obtained as a result of 2D DWT.

There are various types of wavelets that have become widespread during the development of wavelet analysis [25]. One of the wavelets is the Daubechies wavelet, which is frequently used for various applications. Daubechies wavelets are a family of orthogonal wavelets that describe a discrete wavelet transform and are characterized by the maximum number of lost moments for a given support [26]. Each type of wavelet of this class has a scaling function (called the father wavelet) that produces an orthogonal multiresolution analysis. In this study, we calculated the approximation and detail coefficients of the level-2 decomposition of the Daubechies-2 wavelet, and these coefficients were used to combine different phase MR liver images.

Image Fusion

Image fusion is defined as the collection of important features from more than one image, combining them into fewer images, usually a single image. This single image is more informative than any single source image and contains all the necessary information. In computer vision, image fusion is the process of combining relevant information from two or more images into a single image. The resulting image will have more information than any input image [27].

In this study, we use wavelets to combine the four different phases after extracting the features of MR liver images with 2D DWT. The principle of image fusion using wavelets is to combine the wavelet decomposition of images using fusion methods applied to approximation and detail coefficients. For the fusion process, all images must be the same size. For this, images are resized and all phases are scaled to 256x256.

The most preferred image fusion rule using a wavelet transform is the maximum selection rule. In the maximum selection rule, the DWT coefficients of all images are compared and the maximum value between them is selected. While the LL sub-band is an approximation of the input image, the three detail sub-bands provide information about the detail parts LH, HL and HH. The maximum selection rule is applied to the approximation and detail

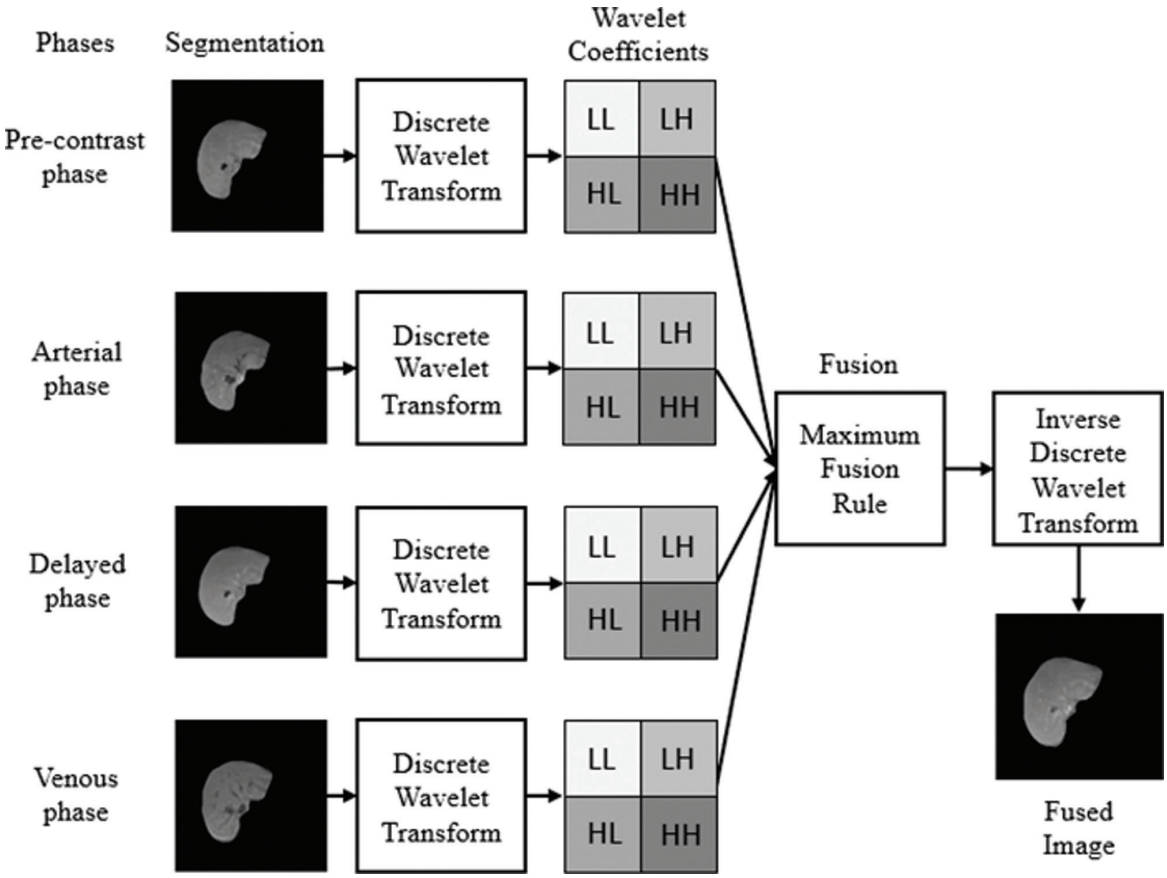

Figure 5. DWT-based fusion method.

sub-bands. The coefficients were obtained for four different phases, and the maximum values between these coefficients were selected. Then, the fused images were created with inverse DWT. The block diagram of the applied fusion method is shown in Figure 5.

The maximum selection rule is shown in Equation 4. Here, A^n corresponds to the approximation coefficients, while D_h^n, D_v^n and D_d^n denote the horizontal, vertical and diagonal detail coefficients, respectively. I_f^n refers to the discrete wavelet coefficients of the fused image. n, corresponds to different patient images.

$$I_f^n = \max\left(A^n, D_h^n, D_v^n, D_d^n\right) \tag{4}$$

Convolutional Neural Networks

The CNNs are a sub-branch of neural networks and are regular versions of multilayer perceptron [28]. CNNs represent feed-forward neural networks consisting of various combinations of convolutional layers, maxpooling layers, and fully connected layers, and exploit spatially local correlation by implementing a local connection model between neurons of adjacent layers. A CNN consists of one or more convolution and maxpooling layers, and eventually ends with a fully connected layer. Today, it is generally used for applications such as image classification, medical image analysis, image clustering and object recognition [29-31]. An example CNN structure is shown in Figure 6. The mathematical equivalent of the 2D CNN process is as follows [32]:

$$v_{ij}^{xy} = f\left(r_{ij} + \sum_{m=0}^{M_i-1}\sum_{h=0}^{H_i-1}\sum_{w=0}^{W_i-1} k_{ijm}^{hw} v_{(i-1)m}^{(x+h)(y+w)}\right) \tag{5}$$

where v refers to the output variable in the property map. H,W represents the size of the filter across the dimension of the data. h,w is the filter index and x is the index of the y feature map. k stands for filter parameters. i,j,m are the indexes of the input layer, output layer and feature map, respectively. M is the number of feature maps, so M_i is i. means the number of feature maps in the layer. r is the bias term.

In this study, CNN is used as a classifier. Convolution layers are used to extract features from the fused images, and the images are reduced in size with maximum pooling layers. The obtained features were then flattened for input to the fully connected layers. The network was made deeper using fully connected layers, and the classification process was completed using the sigmoid activation function. The

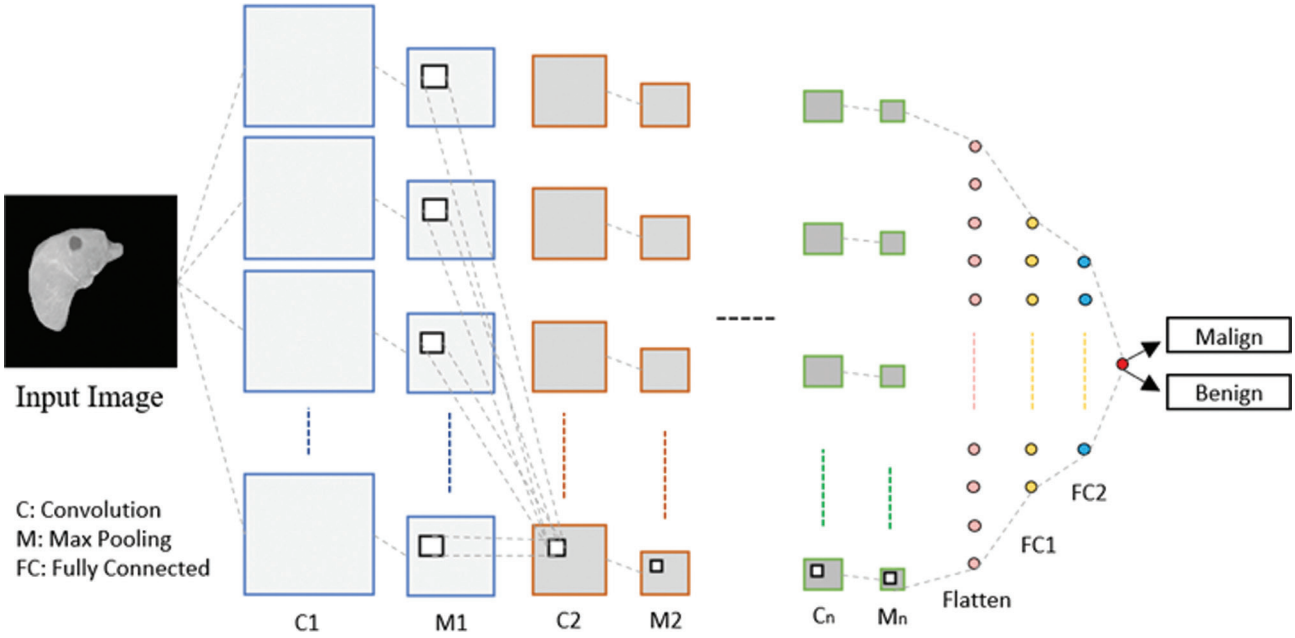

Figure 6. An example of CNN model.

		Predicted class: Positive	Predicted class: Negative
Real class	Positive	TP	FN
	Negative	FP	TN

Figure 7. Confusion matrix representation.

network structure and parameters are explained in detail in the next section.

RESULTS AND DISCUSSIONS

In this study, experiments were carried out to classify malign and benign MR images. To validate the proposed scheme (Figure 1), the simulation was performed on NVIDIA GeForce GTX 1080 Ti, on a workstation with 64 GB of RAM. Additionally, segmentation and image fusion using MATLAB 2020b, training and testing of the CNN model were performed using Python 3.7.3 and Keras 2.3.1 library using the TensorFlow 1.14.0 backend.

To evaluate the results obtained, confusion matrices were created, and sensitivity, specificity and accuracy val-ues were calculated from these matrices. The confusion matrix is a performance evaluation method in which the obtained predict is compared with the real values and is frequently used when evaluating the classification perfor-mance of medical data. Figure 7 shows a representation of the confusion matrix. The confusion matrix represents a two-row and two-column table reporting the number of true positive (TP), false positive (FP), true negative (TN), and false negative (FN). Here, TP and TN show data classified as correct, while FP and FN show data classified as incorrect [33].

Once the confusion matrix is obtained, the classification performance can be evaluated. Using these obtained values, sensitivity (Equation 6), specificity (Equation 7) and accuracy (Equation 8) can be calculated.

- *Sensitivity* calculates the number of malign MR images correctly classified from the total number of malign MR images:

$$Sensitivity = \frac{TP}{TP + FN} \tag{6}$$

- *Specificity* calculates the number of benign MR images correctly classified from the total number of benign MR images:

$$Specificity = \frac{TN}{TN + FP} \tag{7}$$

- *Accuracy* calculates the total number of MR images correctly classified:

$$Accuracy = \frac{TP + TN}{TN + TP + FN + FP} \tag{8}$$

where

- TP: Classification of data belonging to malign class as malign by the system,

- TN: Classification of data belonging to benign class as benign by the system,
- FP: Classification of data belonging to benign class as malign by the system, and
- FN: Classification of data belonging to malign class as benign by the system.

Dataset

In this study, 460 MR liver images from 115 patients in four phases (pre-contrast phase, venous phase, arterial phase and delayed phase) were used. All these images consist of MR liver images with an in-plane resolution of 256x256 in the axial plane. MR liver images were taken from Selcuk University, Faculty of Medicine, Department of Radiology. 20 of the 115 patients have malignant tumors, while 95 of them have benign tumors.

Fusion and CNN Based MR Liver Images Classification

In this study, two experiments were conducted based on the MR liver images classification process. In both experiments, features were automatically extracted from the fused images using convolution layers, and the network was deepened with fully connected layers, and classification was performed using the sigmoid activation function. In addition, to avoid overfitting and to allow the classifier to be generalized to individual datasets, we used 5-fold cross validation. While CNN models were trained in both experiments, 80% of the total data was used for training and 20% for testing. The models trained in 100 epochs. This is because for all experiments, the model was trained approximately one hundred percent. This enabled a more accurate assessment to be made. Batch size was set to 2 as increasing batch size often leads to significant losses in test accuracy [34, 35].

Experiment 1. 115 fusion images (20 malign, 95 benign) were used in Experiment 1. Three different CNN models were created according to the number of convolution layers (number of layers 2, 3 and 4) and these models were trained using the rectified linear unit (Relu), the scaled exponential linear unit (Selu), the exponential linear unit (Elu) and hyperbolic tangent (Tanh) activation functions. The activation function is needed to introduce nonlinear properties to neural networks.

Relu activation function: Relu is one of the most used activation functions in CNNs. For Relu, if the input is positive, the output of Relu is linear, otherwise it is zero. Relu range is (0, ∞). Relu function is continuous, but indistinguishable at x = 0. Since it only uses the max function, the calculation speed is higher compared to other activation functions. Relu function is expressed as in Equation 9, where x is the input tensor.

$$Relu(x) = \max(0, x) \tag{9}$$

Selu activation function: Selu activation function is another variation of Relu. This activation function is generally significantly superior to other activation functions. Selu function is expressed as in Equation 10, where x is the input tensor, and are pre-defined constants (α =1.67 and λ =1.05).

$$Selu(x) = \lambda \begin{cases} x & x > 0 \\ \alpha e^{x} - \alpha & x \leq 0 \end{cases} \tag{10}$$

Elu activation function: Elu is a function that tends to converge cost to zero faster and produce more accurate results. Elu is very similar to Relu except negative inputs. They are both in identity function form for non-negative inputs. Elu function is expressed as in Equation 11, where x is the input tensor, α controls the value to which an Elu saturates for negative net inputs.

$$Elu(x) = \begin{cases} x & x > 0 \\ \alpha\left(e^{x} - 1\right) & otherwise \end{cases} \tag{11}$$

Tanh activation function: Another very popular and widely used activation function is the Tanh. It is a nonlinear function that produces an output in the range of [-1, 1]. Tanh function is expressed as in Equation 12, where x is the input tensor.

$$\mathrm{Tanh}(x) = \frac{e^{2x} - 1}{e^{2x} + 1} \tag{12}$$

As a result of Experiment 1, the best model was determined by comparing the accuracy rates. The obtained results for Experiment 1 are shown in Table 1. According to the table, the best result was achieved using 4 convolution layers and Selu activation function with 83.89% accuracy. The most unsuccessful result was achieved using 4 convolution layers and an Elu activation function of 74.12%. Accuracy rates vary according to the models. This is the proof that no single model can achieve the best result. The best CNN model for Experiment 1 is shown in Figure 8. Due to the limited number of data in this section, the results were relatively low. In the next experiment, it was aimed to obtain better results by increasing the number of data.

Experiment 2. More images are required for effective training of the CNN models. In this experiment, the

Table 1. Results of Experiment 1

Number of Convolution Layer	Accuracy rates (%) using activation functions			
	Relu	***Selu***	***Elu***	***Tanh***
2	82.12	80.52	78.92	81.32
3	74.63	77.32	78.12	75.58
4	77.18	**83.89**	74.12	76.38

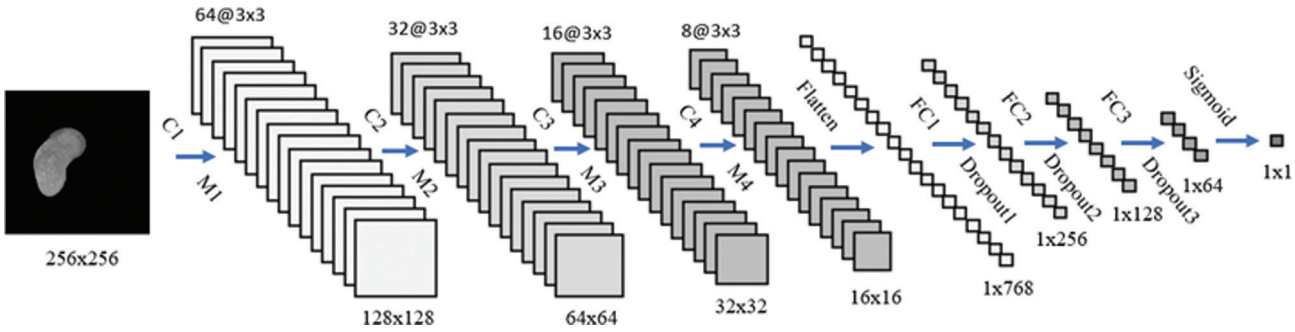

Figure 8. The best CNN model for Experiment 1.

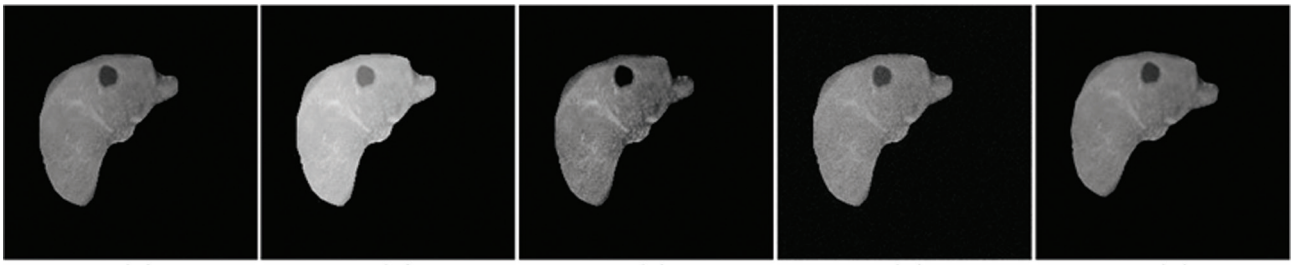

Figure 9. Augmented MR liver fused images: (a) original, (b) brightness enhancement, (c) contrast changing, (d) random noise adding, (e) rotated 10°.

classification was made by increasing the number of data. Data augmentation methods were used to increase the number of data. Data augmentation is a method used to create new data with states that differ from the original data. Brightness enhancement, contrast changes, noise addition and rotation processes were applied as data augmentation methods. Thus, the MR liver images were fivefold augmented (Figure 9). Namely, a total of 575 fused images were used in Experiment 2.

The range of pixel values of the original image in Figure 9 (a) is between 0 and 1. To increase the brightness of the image, 0.25 was added to all pixels, and values greater than 1 were equal to 1. Thus, the range of pixel values was mapped between 0.25 and 1, the resulting image is shown in Figure 9 (b). To change the contrast of the image, all pixels were multiplied by 0.2, resulting in darker images as shown in Figure 9 (c). New images were created by adding random noise to the images as shown in Figure 9 (d). The images were rotated 10 degrees like in Figure 9 (e).

In Experiment 2, the CNN model (Figure 8), which achieved the best result in Experiment 1, was used. Table 2 shows the achieved results for this experiment. This table contains the results obtained using different methods. While classifying with Support Vector Machine (SVM), k-Nearest Neighbors (k-NN) and Artificial Neural Network (ANN) methods, the features of the images are extracted using level-3 2D DWT. Because of the 2D DWT, the image size was reduced to 32x32 and two-dimensional tensors were transformed into one-dimensional tensors, and the obtained 1024 features were given as inputs to the classifiers. Other parameters of the methods are given below.

ANN parameters: Training and testing of the ANN model were performed using Python 3.7.3 and Keras 2.3.1 library. A total of 6 hidden layers are used in the ANN model. There were 512, 256, 128, 64, 32 neurons in these hidden layers, respectively. After each hidden layer, dropout layer and selu activation function were used as in the proposed CNN model. By using a neuron in the output layer, the classification process has been completed with the sigmoid activation function.

SVM parameters: SVM was performed using Python 3.7.3 and Scikit-learn 0.24.2 library. Radial Basis Function (RBF) kernel was used while training the SVM. Here, the *C* parameter was set to *1000* and the gamma kernel coefficient to *0.001* [36].

k-NN parameters: k-NN were performed using Python 3.7.3 and Scikit-learn 0.24.2 library. The number of neighbors has been determined as *5*. Weight function used for prediction was *uniform weights*. Thus, all points in each neighborhood are weighted equally. The *BallTree* algorithm is used to calculate the nearest neighbors. The *Leaf-size* set to 30. *'Minkowski'* was chosen as the distance metric to be used for the tree [37].

Table 2. Results of Experiment 2

Method	Sensitivity	Specificity	Accuracy
SVM	38,57%	89,83%	80,60%
k-NN	33,89%	92,75%	82,16%
ANN	46,66%	96,76%	86,22%
CNN without Fusion	24,58%	84,44%	74,03%
CNN with Fusion	**86,67%**	**98,76%**	**96,66%**

Table 3. Comparison with state-of-the art methods

Other Studies	Classifier	Accuracy
Kabe et al. [1]	CNN	89.20%
Öztürk et al. [9]	ANN	90.00%
Trivizakis et al. [38]	CNN	83.00%
Yasaka et al. [39]	CNN	84.00%
Liang et al. [40]	CNN	87.00%
The proposed method	**CNN**	**96.66%**

According to Table 2, the best result was achieved using the proposed method with 96.66%. Compared with the other results, the proposed method has a superior performance. When the results of CNN with and without fusion are examined, it is seen that the fusion process increases the CNN performance at a high rate. This is an indication that better results will be obtained by fusing images in different phases obtained with MRI instead of using them separately. Additionally, all other methods predicted malign tumors with low accuracy, while the proposed method predicted accuracy as high as 86.67%.

Classification Performance Comparisons

The obtained results were compared with the other classification studies. In the study by Öztürk et al. [9], they made fusion and ANN based classifications using different multiresolution analysis methods. They used the same dataset. There were 3 different fusion rules in this study. In studies using Wavelet Transform, they achieved an average success of 67.78% for 3 different fusion rules. To increase the efficiency of the system, they applied AND/OR operations to the ANN results for each fusion rule and achieved 90% success. Additionally, while malign tumors were detected at a rate of 64.71% in [9], they were detected at a rate of 86.67% in our study. When our study is compared with this study, it shows that CNN achieves better results by extracting more meaningful features with convolution layers compared to ANN. In another study, Trivizakis et al. [38] detected tumors in the liver using CNN. In this study, 83% success was achieved. Compared to our study, it can be seen that the classification performance is low. The result is that after segmenting the liver MRI data, different phases can be combined to obtain more meaningful features and increase CNN performance. Table 3 presents a performance comparison of our model against some state-of-the-art models. When all the studies conducted were examined, the fusion and CNN based method by us achieved higher success than all other methods.

CONCLUSION

One of the most effective ways to classify MR liver images is to use different phase liver images together instead of a single image. Thanks to this method, depending on the phases of the images, many contrast properties can be evaluated together and more realistic results can be obtained.

CNN is a deep learning model that provides high visual performance and is based on applications such as object detection, pattern recognition, segmentation and classification. The features of MR liver images are automatically extracted with the convolution layers within the CNN. Additionally, with fully connected layers, the network is made deeper, and a high accuracy classification result is obtained.

In this study, the classification of liver focal lesions was carried out using CNN. The performance of the proposed method was evaluated by conducting two experiments. In both experiments, the fusion process was performed using 2D DWT. In Experiment 1, it was aimed to find the best CNN model by using the original data. The best result was achieved in this experiment using 4 convolution layers and the Selu activation function. Then, the obtained best model in Experiment 1 was used in Experiment 2. In Experiment 2, first, data was increased, and the CNN model was trained with more data. The number of data was increased 5 times using data augmentation methods. The superiority of the proposed method was proved by comparing it with state-of-the art methods. Our method classified malign with a rate of 86.67% and benign with a rate of 98.76%. For the general accuracy rate, lesions were detected with an accuracy of 96.66%. The obtained results in the experiments CNN with and without fusion were examined, and the positive effect of the fusion process on the performance was observed. Additionally, the results were compared with other studies, and the performance of the proposed method was proven.

ACKNOWLEDGEMENT

The authors would like to thank The Scientific and Technological Research Council of Turkey (TUBITAK) for their support of the project (Project No: 113E184).

AUTHORSHIP CONTRIBUTIONS

Authors equally contributed to this work.

DATA AVAILABILITY STATEMENT

The authors confirm that the data that supports the findings of this study are available within the article. Raw data that support the finding of this study are available from the corresponding author, upon reasonable request.

CONFLICT OF INTEREST

The author declared no potential conflicts of interest with respect to the research, authorship, and/or publication of this article.

ETHICS

There are no ethical issues with the publication of this manuscript.

REFERENCES

[1] Kabe GK, Song Y, Liu Z. Optimization of FireNet for liver lesion classification. Electronics 2020;9:1–16. [CrossRef]

[2] Tajbakhsh N, Shin JY, Gurudu SR, Hurst RT, Kendall CB, Gotway MB, et al. Convolutional neural networks for medical image analysis: Full training or fine tuning? IEEE Trans Med Imaging 2016;35:1299–1312. [CrossRef]

[3] Rofsky NM, Lee VS, Laub G, Pollack MA, Krinsky GA, Thomasson D, et al. Abdominal MR imaging with a volumetric interpolated breath-hold examination. Radiology 1999;212:876–884. [CrossRef]

[4] Low RN. Abdominal MRI advances in the detection of liver tumours and characterization. Lancet Oncol 2007;8:525–535. [CrossRef]

[5] Galea N, Cantisani V, Taouli B. Liver lesion detection and characterization: Role of diffusion-weighted imaging. J Magn Reason Imaging 2013;37:1260–1276. [CrossRef]

[6] Li Z, Mao Y, Huang W, Li H, Zhu J, Li W, et al. Texture-based classification of different single liver lesion based on SPAIR T2W MRI images. BMC Med Imaging 2017;17:42.

[7] Niraj LK, Patthi B, Singla A, Gupta R, Ali I, Dhama K, et al. MRI in dentistry- A future towards radiation free imaging - systematic review. J Clin Diagn Res 2016;10:14–19. [CrossRef]

[8] Albiin N. MRI of focal liver lesions. Curr Med Imaging 2012;8:107–116. [CrossRef]

[9] Ozturk AE, Ceylan M. Fusion and ANN based classification of liver focal lesions using phases in magnetic resonance imaging. 2015 IEEE 12th International Symposium on Biomedical Imaging (ISBI); 2015 Apr 16–19; Brooklyn, USA: IEEE; 2015. pp. 415–419. [CrossRef]

[10] Morlet J, Arens G, Fourgeau E, Giard D. Wave propagation and sampling theory-part II: Sampling theory and complex waves. Geophysics 1982;47:222–236. [CrossRef]

[11] Mojsilovic A, Popovic M, Sevic D. Classification of the ultrasound liver images with the 2N/spl times/1-D wavelet transform. Proceedings of 3rd IEEE International Conference on Image Processing; 1996 Sept 16-19; Lausanne, Switzerland: IEEE; 1996. pp. 367–370.

[12] Beura S, Majhi B, Dash R. Mammogram classification using two dimensional discrete wavelet transform and gray-level co-occurrence matrix for detection of breast cancer. Neurocomputing 2015;154:1–14. [CrossRef]

[13] Uppal MTN. Classification of mammograms for breast cancer detection using fusion of discrete cosine transform and discrete wavelet transform features. Biomed Res 2016;27:322–327.

[14] Sarhan AM. Brain tumor classification in magnetic resonance images using deep learning and wavelet transform. J Biomed Eng 2020;13:102–112. [CrossRef]

[15] Yoshida H, Keserci B, Casalino DD, Coskun A, Ozturk O, Savranlar A. Segmentation of liver tumors in ultrasound images based on scale-space analysis of the continuous wavelet transform. 1998 IEEE Ultrasonics Symposium; 1998 Oct 5-8; Sendai, Japan: IEEE; 1998. pp. 1713–1716.

[16] Kutlu H, Avcı E. A novel method for classifying liver and brain tumors using convolutional neural networks, discrete wavelet transform and long short-term memory networks. Sensors 1992;19:1–16. [CrossRef]

[17] Abd El Kader I, Xu G, Shuai Z, Saminu S, Javaid I, Salim Ahmad I. Differential deep convolutional neural network model for brain tumor classification. Brain Sci 2021;11:352. [CrossRef]

[18] Alakwaa W, Nassef M, Badr A. Lung cancer detection and classification with 3D convolutional neural network (3D-CNN). Int J Adv Comput Sci Appl 2017;8:409–417. [CrossRef]

[19] Alkhaleefah M, Wu CC. A hybrid CNN and RBF-based SVM approach for breast cancer classification in mammograms. 2018 IEEE International Conference on Systems, Man, and Cybernetics (SMC); 2018 Oct 7-10; Miyazaki, Japan: IEEE; 2018. pp. 894–899. [CrossRef]

[20] Frid-Adar M, Diamant I, Klang E, Amitai M, Goldberger J, Greenspan H. GAN-based synthetic medical image augmentation for increased CNN performance in liver lesion classification. Neurocomputing 2018;321:321–331. [CrossRef]

[21] Li J, Liang B, Wang Y. A hybrid neural network for hyperspectral image classification. Remote Sens Lett 2020;11:96–105. [CrossRef]

[22] Jiang X, Chang L, Zhang YD. Classification of Alzheimer's disease via eight-layer convolutional

neural network with batch normalization and dropout techniques. J Med Imaging & Health Infor 2020;10:1040–1048. [CrossRef]

[23] Elgendi M, Nasir MU, Tang Q, Smith D, Grenier JP, Batte C, et al. The effectiveness of image augmentation in deep learning networks for detecting COVID-19: A geometric transformation perspective. Front Med 2021;8:1–12. [CrossRef]

[24] Ceylan M, Ozbay Y, Yıldırım E. A new approach for biomedical image segmentation: Combined complex-valued artificial neural network case study: Lung segmentation on chest CT images. 5th Cairo International Biomedical Engineering Conference; 2010 Dec 16-18; Cairo, Egypt: IEEE; 2010. pp. 33–36. [CrossRef]

[25] Nayak DR, Dash R, Majhi B. Brain MR image classification using two-dimensional discrete wavelet transform and AdaBoost with random forests. Neurocomputing 2016;177:188–197. [CrossRef]

[26] Deepa R, Rajaguru H, Babu CG. Analysis on wavelet feature and softmax discriminant classifier for the detection of epilepsy. ICCSSS 2020: First International Conference on Circuits, Signals, Systems and Securities; 2020 Dec 11-12; Tamil Nadu, India: IOP Science; 2020. 012036. [CrossRef]

[27] Haghighat MBA, Aghagolzadeh A, Seyedarabi H. Multi-focus image fusion for visual sensor networks in DCT domain. Comput Electr Eng 2011;37:789–797. [CrossRef]

[28] Cihan M, Ceylan M. NE3D-CNN: A new 3D convolutional neural network for hyperspectral image classification and remote sensing application. Eur J Lipid Sci Technol, 65–71.

[29] Sun Y, Xue B, Zhang, M, Yen GG. Evolving deep convolutional neural networks for image classification, IEEE Transactions on Evolutionary Computation 2009;24(2):394–407. [CrossRef]

[30] Zhang YD, Dong Z, Chen X, Jia W, Du S, Muhammad K, et al. Image based fruit category classification by 13-layer deep convolutional neural network and data augmentation. Multimed Tools Appl 2019;78:3613–3632. [CrossRef]

[31] Cihan M, Ceylan M, Ornek AH. Spectral-spatial classification for non-invasive health status detection of neonates using hyperspectral imaging and deep convolutional neural networks. Spectrosc Lett 2022;55:336–349. [CrossRef]

[32] He M, Li B, Chen H. Multi-scale 3D deep convolutional neural network for hyperspectral image classification. 2017 IEEE International Conference on Image Processing (ICIP); 2017 Sept 17-20; Beijing, China: IEEE; 2017. pp. 3904–3908. [CrossRef]

[33] Cihan M, Ceylan M, Soylu H, Konak M. Fast evaluation of unhealthy and healthy neonates using hyperspectral features on 700-850 Nm wavelengths, ROI extraction, and 3D-CNN. IRBM 2022;43:362–371. [CrossRef]

[34] Goyal P, Dollár P, Girshick R, Noordhuis P, Wesolowski L, Kyrola A, et al. Accurate, large minibatch sgd: Training imagenet in 1 hour, 2017.

[35] Hoffer E, Hubara I, Soudry D. Train longer, generalize better: Closing the generalization gap in large batch training of neural networks. Adv Neural Inf Process Syst 2017;30:1729–1739.

[36] Parisi L. M-arcsinh: An Efficient and Reliable Function for SVM and MLP in scikit-learn, 2020.

[37] Hackeling G. Mastering Machine Learning with Scikit-Learn. 2nd ed. Birmingham: Packt Publishing; 2017.

[38] Trivizakis E, Manikis GC, Nikiforaki K, Drevelegas K, Constantinides M, Drevelegas A, et al. Extending 2-D convolutional neural networks to 3-D for advancing deep learning cancer classification with application to MRI liver tumor differentiation. IEEE J Biomed Health Inform 2019;23:923–930. [CrossRef]

[39] Yasaka K, Akai H, Abe O, Kiryu S. Deep learning with convolutional neural network for differentiation of liver masses at dynamic contrast-enhanced CT: A preliminary study. Radiology 2018;286:887–896. [CrossRef]

[40] Liang D, Lin L, Hu H, Zhang Q, Chen Q, Han X, et al. Residual convolutional neural networks with global and local pathways for classification of focal liver lesions. In: Geng X, Kang BH, editors. Pacific Rim International Conference on Artificial Intelligence; 2018 Aug 28-31; Nanjing, China: Springer; 2018. pp. 617–628. [CrossRef]